

Geophysical Research Letters[®]



RESEARCH LETTER

10.1029/2023GL104046

Key Points:

- The variation range of Jovian subsolar magnetopause standoff distance is very large even under constant solar wind conditions
- Interchange structures in the Jovian magnetodisc may affect the location of the magnetopause
- Significant radial dynamic pressure inside the Jovian magnetosphere may be the root cause of the variations of magnetopause

Supporting Information:

Supporting Information may be found in the online version of this article.

Correspondence to:

B. Zhang and E. Feng,
binzh@hku.hk;
fengenh@connect.hku.hk







Citation:

Feng, E., Zhang, B., Yao, Z., Delamere, P. A., Zheng, Z., Dunn, W. R., & Ye, S.-Y. (2023). Variation of the Jovian magnetopause under constant solar wind conditions: Significance of magnetodisc dynamics. *Geophysical Research Letters*, 50, e2023GL104046. <https://doi.org/10.1029/2023GL104046>

Received 8 APR 2023

Accepted 1 JUN 2023

Variation of the Jovian Magnetopause Under Constant Solar Wind Conditions: Significance of Magnetodisc Dynamics

Enhao Feng^{1,2} , Binzheng Zhang² , Zhonghua Yao^{2,3} , Peter A. Delamere⁴ , Zhiqi Zheng² , William R. Dunn⁵ , and Sheng-Yi Ye⁶

¹Department of Physics, the University of Hong Kong, Pokfulam, Hong Kong SAR, ²Department of Earth Sciences, the University of Hong Kong, Pokfulam, Hong Kong SAR, ³Institute of Geology and Geophysics, Chinese Academy of Sciences, Beijing, China, ⁴Department of Physics, University of Alaska Fairbanks, Fairbanks, AK, USA, ⁵Department of Physics and Astronomy, University College London, London, UK, ⁶Department of Earth and Space Sciences, Southern University of Science and Technology, Shenzhen, China

Abstract It is generally believed that variations in the upstream solar wind (SW) and interplanetary magnetic field (IMF) conditions are the main cause of changes of Jupiter's magnetopause (JM) location. However, most previous pressure balance models for the JM are axisymmetric and do not consider internal drivers, for example, the dynamics of the magnetodisc. We use three-dimensional global magnetosphere simulations to investigate the variation of the JM under constant SW/IMF conditions. These simulations show that even without variations in the upstream driving conditions, the JM can exhibit dynamic variations, suggesting a range as large as 50 Jupiter radii in the subsolar location. Our study shows that the interchange structures in the Jovian magnetodisc will introduce significant radial dynamic pressure, which can drive significant variation in the JM location. The results provide important new context for interpreting the JM location and dynamics, with key implications for other internally mass-loaded and/or rapidly rotating systems.

Plain Language Summary The location of Jupiter's magnetopause is impacted by both external and internal conditions. In observations, the location of Jupiter's magnetopause has been found to change greatly and rapidly. This variation is generally believed to be caused by the significant changes in the external conditions. However, to-date models and simulations have been mostly axisymmetric and static for the internal environment. Therefore, today, there is no interpretation that the internal mechanisms are sufficient to drive the drastic variation of Jupiter's magnetopause. In fact, because of the rapid rotation of Jupiter, as well as the particle outflow caused by volcanism on Jupiter's moon Io, the internal environment of Jupiter's magnetosphere is quite active. It is possible that the activity of the internal magnetospheric environment has a greater impact on Jupiter's magnetopause. We used three-dimensional global simulations to investigate the variation of Jupiter's magnetopause under constant external conditions. The results show that even under constant external conditions, Jupiter's magnetopause will be highly impacted by internal conditions. Our study reveals the importance of the internal magnetospheric environment for the variation of Jupiter's magnetopause, even the whole magnetospheric system.

1. Introduction

The Jovian magnetopause, which is the boundary of the Jovian magnetosphere, is one of the most important physical regions for understanding giant magnetospheres. Based on existing knowledge on the configuration of planetary magnetospheres, the upstream solar wind (SW) conditions determine the size and shape of a magnetosphere, that is, the location of the magnetopause (e.g., Huddleston et al., 1998). For example, it is believed that the decrease of the Jovian standoff distance is a consequence of magnetospheric compression caused by enhanced SW dynamic pressure (e.g., Ebert et al., 2014; Joy et al., 2002; McComas et al., 2014). However, if only considering the balance between SW dynamic pressure and magnetic pressure without the contribution of the plasma sheet, the predicted standoff distance is only about 42 Jupiter Radii (R_J) under nominal upstream conditions, which is much smaller compared with observations (e.g., Bame et al., 1992; Delamere & Bagenal, 2010; Desroche et al., 2012; Kivelson et al., 1997; Lepping et al., 1981; Wolfe et al., 1974). To reconcile this inconsistency in the Jovian magnetosphere, the hot plasma populations (e.g., Krimigis et al., 1979; Krimigis et al., 1981), and the equatorial current sheet or magnetodisc were considered in theoretical or empirical models and numerical simulations (e.g., Alexeev & Belenkaya, 2005; Aoyama & Oya, 1985; Engle & Beard, 1980; Khurana, 1997;

© 2023. The Authors.

This is an open access article under the terms of the [Creative Commons Attribution License](https://creativecommons.org/licenses/by/4.0/), which permits use, distribution and reproduction in any medium, provided the original work is properly cited.

Ogino et al., 1998; Stahara et al., 1989), which have shown much larger standoff distances that are more consistent with observations. However, these previous studies are either based on an axisymmetric Jovian magnetosphere model or a static Jovian magnetodisc picture. Recent observational studies have shown that the Jovian magnetosphere exhibits significant spatial and temporal variations, indicating that structure due to the internal dynamics of the Jovian space plasma may have an important role in regulating the shape of the giant magnetosphere (Gu et al., 2023; Schok et al., 2023).

The rapid variations of the location of the Jovian magnetopause have been seen in previous and on-going in-situ observations. For example, during the first three apoJove periods, the Juno spacecraft was found to cross the magnetopause (dawn flank) more than 97 times in the range of 73 to 114 R_J (Hospodarsky et al., 2017). It is generally believed that the drastic change of the SW dynamic pressure will cause the variation of the magnetopause standoff distance (e.g., Ebert et al., 2014; Huddleston et al., 1998; Joy et al., 2002; McComas et al., 2014; Slavin et al., 1985). With recent studies on the dynamic variation associated with density structures in the Jovian magnetosphere (e.g., Huscher et al., 2021; Schok et al., 2023; Wang et al., 2023), question remains how important internal dynamics are on the variations of the magnetopause.

Using Juno-JADE measurements, Huscher et al. (2021) have shown that the magnetodisc density profiles are quite variable in small structures, from orbit to orbit. The variations of the magnetodisc current and outward radial currents on the equatorial plane may influence the transfer of angular momentum to outward flowing plasma (Connerney et al., 2020). Schok et al. (2023) found that there would be magnetic field fluctuations with 1–10 hr periodicities near dawn/tail flank and the magnetodisc. Thus, the static assumption is questionable, and internal variations within the Jovian magnetosphere cannot be completely ignored for predicting the Jovian magnetopause. Such dynamic characteristics are also seen in auroral activities, such as variations of Jupiter's ultraviolet aurora (Grodent et al., 2018), auroral dawn storms (Bonfond et al., 2021) and auroral injections (e.g., Yao et al., 2020). Moreover, the internal magnetospheric dynamics may also result in explosive activities such as magnetic loading/unloading process in the middle magnetosphere (Yao et al., 2019), influencing the global configuration of the Jovian magnetosphere. Structures in Jupiter's X-ray aurorae, which map to the outer magnetosphere and have been proposed to relate to processes near the magnetopause also exhibit substantial spectral, temporal, and spatial variability during intervals of seemingly quiescent solar wind (Dunn et al., 2020). A recent study has also found that interchange structures within the magnetodisc greatly influence the reconnection in the region from magnetotail to dawn side, resulting in significant variations in the middle-outer magnetosphere with a significant increase in the auroral Alfvénic power (Feng et al., 2022). This series of observational evidence suggests that the Jovian magnetopause may not be described accurately by existing axial symmetric, simple pressure balance models, and the influence from the internal dynamics needs to be considered when studying giant magnetospheres.

Previous work has shown the importance of internal conditions for the compressibility, dayside shape and size of the magnetopause in Saturn or Jupiter (Achilleos et al., 2021; Hardy et al., 2020; Pilkington et al., 2015). In the magneto-hydrodynamics (MHD) models, variations of the magnetopause in Saturn and Jupiter have also been shown (Chané et al., 2017; Jia et al., 2012).

To quantify the impact from internal drivers on the variation of the Jovian magnetopause, we use global magnetospheric simulations to investigate the variation of the magnetopause under nominal, time-steady SW conditions near Jupiter's orbit. By excluding the variations in the upstream driving conditions, we show that the variation range of the Jovian magnetopause location is very large, and the interchange structures within the magnetodisc regulate the shape of the magnetopause. These results provide a new perspective on understanding the configuration of the Jovian magnetosphere. The paper is organized as follows: Section 2 describes the simulation setup; Section 3 describes the simulation results, and Section 4 discusses the internal mechanism of magnetopause variations.

2. Simulation Information

The numerical simulations are based on the global Jovian magnetosphere model developed by Zhang et al. (2021) and the MHD equations are solved using the Grid Agnostic MHD for Extended Research Applications (GAMERA) code (Zhang, Sorathia, Lyon, Merkin, & Wiltberger, 2019; Zhang, Sorathia, Lyon, Merkin, Garretson, & Wiltberger, 2019). The code solves the MHD equations on a non-orthogonal, curvilinear grid adapted to Jovian

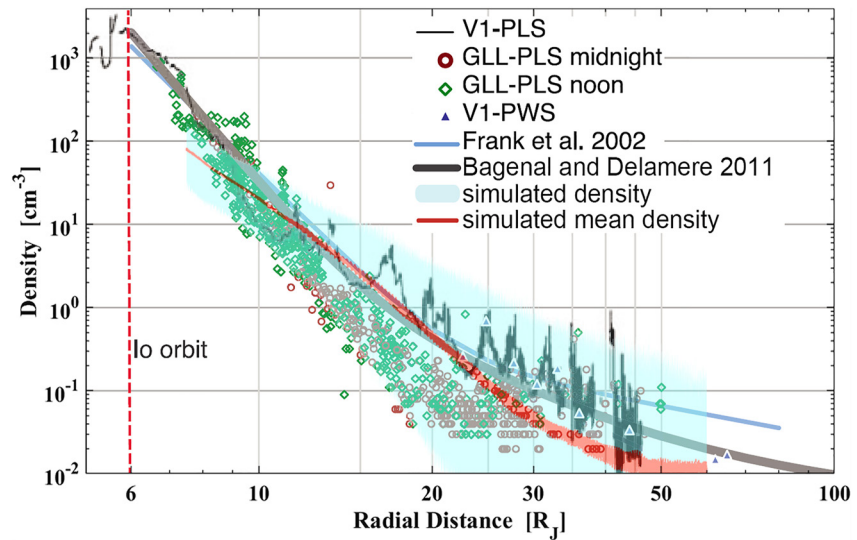


Figure 1. The average radial density profile of the simulation, compared with Figure 1 from Bagenal and Delamere (2011). The cyan shadow represents the simulated density distribution and the red line represents the simulated mean density.

magnetospheric problems based on finite-volume techniques. In the solar-magnetic (SM) coordinate system, a stretched spherical grid extends to $120 R_J$ in the sunward direction, $-1300 R_J$ in the anti-sunward direction, and $\pm 360 R_J$ in the directions perpendicular to the sun-Jupiter axis. The grid is spherical polar near the low-altitude (inner) boundary with the axis of symmetry along the SM x -axis. The grid resolution is highly non-uniform with $\Delta r = 0.6 R_J$ in the radial direction near the simulated dayside magnetopause, and approximately $\Delta r = 0.15 R_J$ near the inner boundary, which is set to be a spherical shell at $3.5 R_J$ Jovi-centric. The time resolution of the simulation data output is 120 s, which is sufficient to resolve the temporal variation in the Jovian magnetopause. A dipole placed at the origin of SM is used to represent the Jovian intrinsic magnetic field in the simulation, and the tilt angle is ignored in the following numerical experiments. This is for the simplification of analysis because it is convenient for us to study the effect of magnetodisc on magnetopause by excluding the asymmetry of the intrinsic magnetic field.

To implement the rapid rotation of Jupiter, a corotation potential after the electrostatic magnetosphere-ionosphere coupling (Merkin & Lyon, 2010) is imposed. To implement Iogenic mass loading, we use the following simple spatial function representing the density distribution of the Io plasma torus:

$$\Delta n = A e^{-k \times R_d}, \quad (1)$$

where Δn in Equation 1 is the volumetric Iogenic source rate (in cm^{-3}/s), and the parameter A is used to control the total rate of mass loading. R_d is the minimum distance between any point (x, y, z) and the orbit of Io ($6 R_J$ Jovi-centric in the simulation):

$$R_d = ((r_e - 6)^2 + z^2)^{1/2} \quad 5R_J \leq r_e \leq 8R_J, |z| \leq 1R_J, \quad (2)$$

with $r_e = (x^2 + y^2)^{1/2}$ is the equatorial radius for any given location (x, y, z) . In the following simulations, we use $A = 280$ and $k = 7$, which gives a fixed Io mass loading rate of approximately 1,100 kg/s. Numerical experiments have shown that the value of parameter k has little effect on the simulation results when $k \geq 3$, especially the radial density profile. The mass loading process is switched on at 00:00 simulation time (ST) with a fixed rate throughout the entire simulation. The magnitude of the interplanetary magnetic field (IMF) is fixed as $B_x = B_z = 0$, $B_y = 0.3 \text{ nT}$. The speed of SW was set to be $V_x = 360 \text{ km/s}$, $V_y = V_z = 0$, and the density of SW was $0.18/\text{cc}$, which are near the median or mean values of SW proton speed and density measured at 5AU (e.g., Ebert et al., 2014; Jackman & Arridge, 2011).

The simulation was run for approximately 300 hr in order to reach a quasi-balanced state, in which the radial density profile within the magnetodisc remains approximately the same in a local-time averaged sense. Figure 1

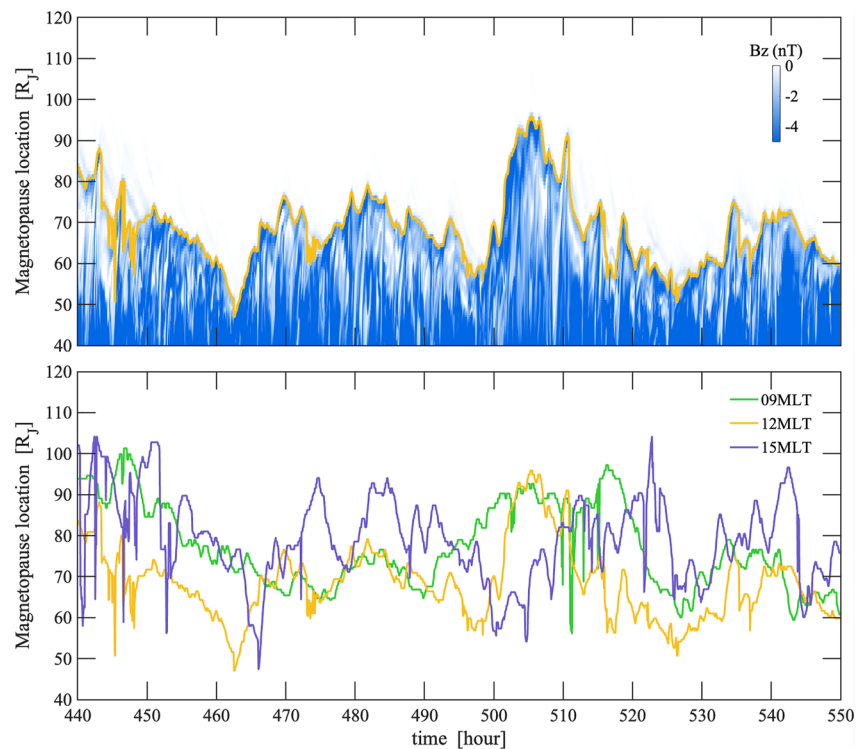


Figure 2. Top panel show the B_z component near 12 MLT, and the bottom panel show the variations of the magnetopause near 9, 12, and 15 MLT.

demonstrates the effectiveness of the global Jovian magnetosphere model in reproducing the observed plasma number density profile within the magnetodisc. The simulated radial density profile in the simulation is shown together with in-situ measurements and empirical distributions from Bagenal and Delamere (2011). The simulated density profiles are in excellent agreement with observation especially in the middle magnetosphere between 8 and 50 R_j . Thus, the numerical experiments are suitable for investigating the internal driver of the Jovian magnetosphere. Note that we have not yet implemented the hot plasma population in our global simulations, which may cause the simulated magnetosphere to be a bit smaller, but the absence of a hot plasma component does not affect the conclusions of this paper. The total simulation time is about 550 hr and the interval from ST = 440–550 hr is used in the following analysis.

Since no tilt is introduced in the simulation and the upstream IMF is in the y -direction, the location of the equatorial magnetopause is found by tracking the boundary where the magnetic field switches from B_z to B_y along the equatorial plane. This algorithm of tracking the magnetopause boundary works well in the equatorial plane, because the B_z component in the magnetosheath and IMF is essentially zero. Examples of the variation and boundary of B_z jump are clearly seen in the top right panel of Movies S1–S3. In the following analysis we only focus on the location of the magnetopause boundary in the equatorial plane.

3. Results

Figure 2 shows the spatial and temporal variation of the simulated magnetopause location during ST = 440–550 hr. The top panel in Figure 2 show the temporal variation of the B_z component along 12 MLT in the equatorial plane. The boundary of the B_z jump is marked using a thick yellow line, which is defined as the location of the magnetopause. The bottom panel show the temporal variations of the equatorial magnetopause at 9, 12 and 15 MLT. At 9 MLT, the location of the equatorial magnetopause exhibits a range between 57 and 101 R_j , while the location of the subsolar magnetopause varies in the range of 47 to 95 R_j . Among the three selected MLTs, the largest range of variation is near 15 MLT, which is between 48 and 104 R_j . In addition, the periodicity of the variation (local maximum or minimum appears) is roughly about once per 1–2 hr, which is higher than the rotation period of Jupiter.

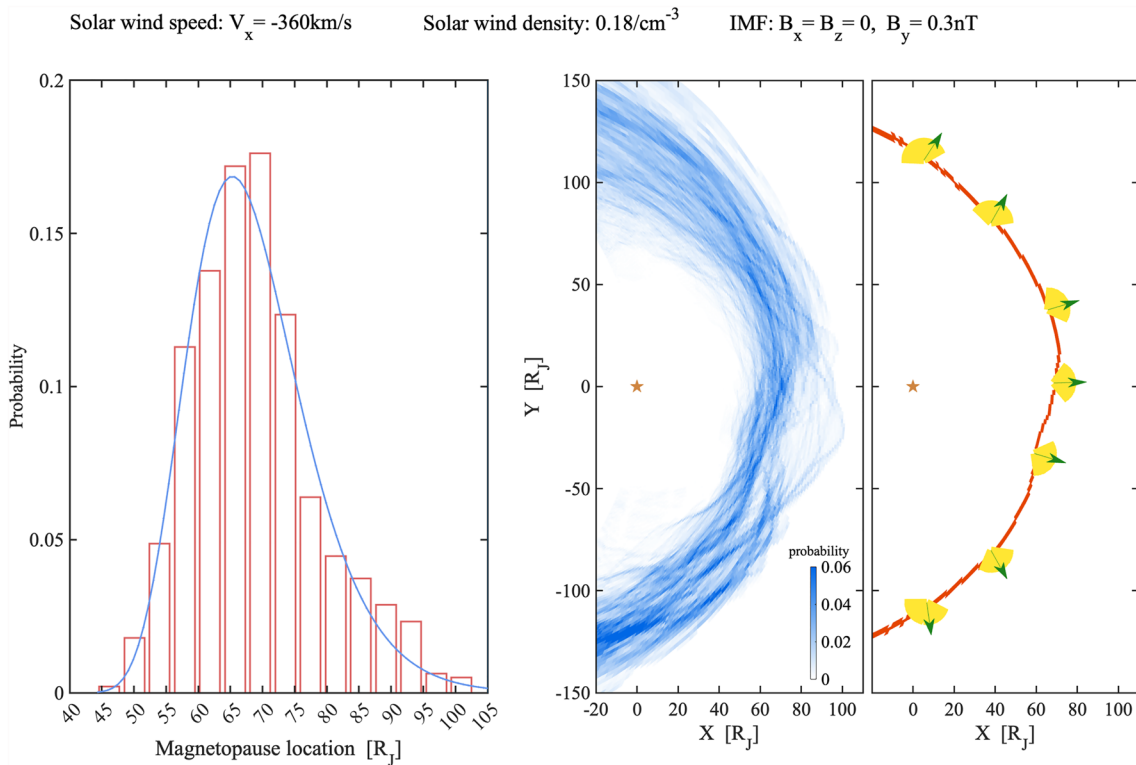


Figure 3. Left panel shows the statistical results of the magnetopause data near noon (11, 12, 13 MLT). The blue line is a log-normal fitting. Middle panel shows the probability distribution of magnetopause, and right panel shows the expected location of the magnetopause in the X-Y plane (red line), the expected normal direction to the magnetopause (green arrow), and range of variation in the expected normal direction (yellow sector). The brown stars mark the location of Jupiter.

The left panel in Figure 3 is a histogram showing the spread of the simulated equatorial magnetopause locations near noon (including 11, 12, 13 MLT). Driven by the nominal SW/IMF conditions used in the simulation, the mean location of the subsolar magnetopause is between 65 and 70 R_J , which is significantly greater than the 42 R_J predicted by simple pressure balance model.

Moreover, it is evident that even though the upstream driving condition is constant over time, the variation of the subsolar magnetopause location is unexpectedly large, ranging from 44 to 103 R_J , which is not predicted by existing pressure balance models.

The middle panel in Figure 3 shows the probability distribution of the simulated equatorial magnetopause driven by steady-state upstream SW/IMF conditions. The probability distribution was calculated along each direction over the sampling period $ST = 440\text{--}550$ hr. The spatial variation of the equatorial magnetopause location is clearly seen in the probability distribution. Near the dawn flank, the location of magnetopause can vary from 80 R_J to approximately 140 R_J , while near the dusk flank, the variation range is mostly between 70 and 150 R_J , with extreme cases beyond 160 R_J . The right panel in Figure 3 shows the expectation of equatorial magnetopause (the red line), the average normal direction of magnetopause (the green arrows) and the corresponding range of variation (the yellow sectors) in the boundary normal direction. In the simulation driven by steady-state upstream conditions, the range of variation in the magnetopause boundary normal direction is quite large, which exceeds 90° near 12 MLT. In the dawn and dusk flank sectors, the variations are even larger. Note that as shown in the right panel of Figure 3, the normal direction of the equatorial magnetopause at dawn and dusk flank (the bottom and top yellow sectors) can be directed toward the nightside, which means that the magnetopause near these regions can have a large bend. This kind of large bend can be found in the top right panel in Figure S1 in Supporting Information S1. These unusual normal directions of the equatorial magnetopause suggest that the instantaneous Jovian magnetosphere boundary may have very irregular shapes that again cannot be described by existing static, simple geometric models of the Jovian magnetopause.

Figure 4 shows two snapshots from the simulation at $ST = 501.6$ and 519.0 hr, displaying the instantaneous distributions of density, plasma β and radial dynamic pressure (ρv_r^2) in the equatorial plane. The left, middle and right panels are the density ρ , plasma β and ρv_r^2 , respectively, where v_r is the radial bulk velocity. Interchange structures

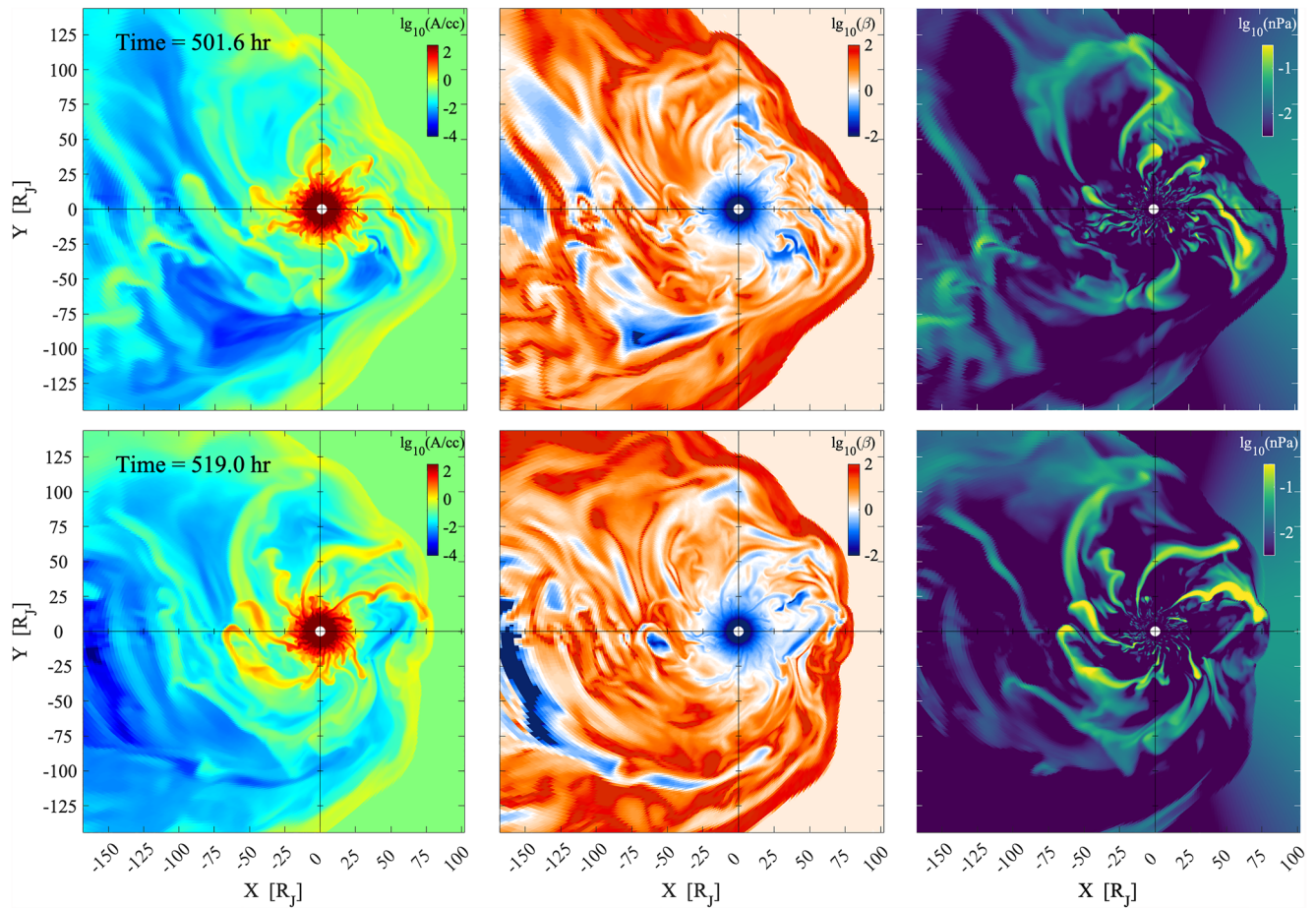


Figure 4. The distributions of density (left panels), plasma β (middle panels) and ρv_r^2 (right panels) for ST = 501.6 hr (top panels) and 519.0 hr (bottom panels).

in the simulated Jovian magnetosphere is evident in the local density enhancements. These interchange structures, which have different spatial variations, are generated due to interchange instabilities in the inner magnetodisc, transporting plasma radially outward to the middle and outer magnetosphere and interacting with the Jovian magnetopause. Note that these magnetospheric structures may evolve to very complicated structures in the outer magnetosphere, resulting in filamentary structures. Moreover, the right panels of Figure 4 show that these interchange structures have very high radial dynamic pressure ρv_r^2 that cannot be ignored in a magnetopause pressure balance model. For example, the instantaneous radial dynamic pressure of the interchange structures near the noon sector is mostly in the range of 0.5–2 nPa, which is much higher than the SW dynamic pressure (about 0.04 nPa) set in the simulation. In addition to Figure 4, the radial dynamic pressure can be seen in Movies S1–S3.

4. Discussion

Juno observations have shown that the Jovian magnetopause is much more dynamic than expected (Bagenal et al., 2017). For example, during the first three apojoVe periods, more than 97 magnetopause crossings have been identified on the dawn flank (Hospodarsky et al., 2017). It is generally believed that the planetary magnetopause is controlled by the upstream SW/IMF variations. Our study suggests that the internal dynamics of the fast-rotating Jovian magnetodisc may have a significant impact on the shape of the Jovian magnetopause. Under constant, nominal SW/IMF conditions, the variation of the standoff distance in the noon sector may be more than 50 R_J , which is not predicted by existing theoretical/empirical models of the Jovian magnetopause. The temporal variation of the magnetopause boundary has periodicities around a few hours, which is similar to the characteristic periodicity of ultralow-frequency waves in the magnetosheath (Gu et al., 2023) and the periodicity of plasma density variations in the dawnside magnetosphere (Schok et al., 2023).

The pattern of simulated magnetopause variations can show different magnetopause crossing (MC) time intervals, which can be from tens of minutes to 2 hr, or from a few hours to more than ten hours. These time intervals are consistent with the different time intervals of Juno MC shown in Table S2 by Hospodarsky et al. (2017). For example, in bottom panel of Figure 2, considering a horizontal line at 75 R_J , there are about 9 intersections between the horizontal line and the line of magnetopause location at 9 MLT within $ST = 458\text{--}465$ hr (9 crossings/7 hr), which means that if a spacecraft stays at this location, MC can be found every 1–2 hr, or even every tens of minutes, as shown in Table S2 by Hospodarsky et al. (2017). On the other hand, considering a spacecraft stays near 85 R_J at dawn, there are only six crossings within $ST = 445\text{--}505$ hr (6 crossings/60 hr) according to Figure 2. For the Juno spacecraft, many MCs with time intervals from 3 hr to more than 10 hr can also be found in Hospodarsky et al. (2017). It is important to note that, even though the simulated MCs are consistent with the time scales in Hospodarsky et al. (2017), single spacecraft measurements of MCs are not sufficient to rule out the influence from the variations in the upstream conditions. For example, during a SW compression period, MC may not occur as the spacecraft stays relatively far away. Even so, the variation frequencies of the magnetopause in our simulation indicates that even under constant SW/IMF conditions, various MC time intervals can still occur, which is consistent with the various MC intervals of Juno. Thus, further analysis combined with more in-situ observations and modeling is needed to quantify the influence of the external factors.

The bimodal distribution of the Jovian magnetopause shown in Joy et al. (2002) was mainly due to the bimodal distribution of the SW parameters used in driving their model. It is not yet conclusive whether the distribution of SW conditions near Jupiter exhibit bimodal or other specific features (Ebert et al., 2014). Our simulation results show local bimodal or even trimodal distribution under constant SW conditions. For example, as shown in middle panel of Figure 3, there is a local bimodal-like distribution near 9 MLT, and a local trimodal-like distribution near 8 MLT. Overall, the questions whether or how such local bimodal or multimodal distributions depends on internal conditions and/or external drivers are out of the scope of this study and require future investigation.

Moreover, the shape of the magnetopause also exhibits dynamic features that are not expected in standard, parabolic-like planetary magnetopause models. For example, the instantaneous magnetopause may have a very large bend near dawn and dusk sides, with normal directions pointing toward the nightside. Note that the Kelvin-Helmholtz instability can also deform the magnetopause boundary to a certain extent (Ma et al., 2022; Zhang et al., 2018). However, the large-scale deformations shown in our simulation should be primarily driven by the dynamics of the interchange structures. These new simulation results indicate that unlike the terrestrial magnetosphere, the shape of a fast-rotating giant magnetosphere may be largely regulated by internal dynamics rather than by upstream driving conditions, due to the evolution of interchange structures in the magnetodisc.

The radial transport associated with the interchange structures in the magnetodisc is critical in regulating the boundary of the fast-rotating Jovian magnetosphere. In the simulation, because of the existence of interchange instability (e.g., Achilleos et al., 2015 and references therein), there will be plasma transport process from inside to outside, which generates the interchange structure. The interchange instability is caused by the perturbation of plasma due to the influence of gravitational force, centrifugal force, pressure gradient and magnetic tension force. When the system reaches a quasi-balanced state (e.g., $ST \sim 300$ hr), the non-linear evolution of these interchange structure continues transporting plasma radially outward, causing spatial and temporal variations in the boundary when these structures interact with the magnetopause.

When the interchange structures interact with the magnetopause boundary, the corresponding radial dynamic pressure is in the range of 0.5–2 nPa. Compared to the SW ram pressure (about 0.04 nPa) in the simulation, the radial dynamic pressure due to these interchange structures is sufficient to drive the variation of the magnetopause. According to the momentum equation of magnetospheric plasma:

$$\partial \rho \mathbf{u} / \partial t = -\nabla \cdot \left[\rho \mathbf{u} \mathbf{u} + \bar{\mathbf{I}}(P + B^2/2) - \mathbf{B}\mathbf{B} \right] \quad (3)$$

where ρ is the plasma mass density, \mathbf{u} is the plasma bulk velocity, $\bar{\mathbf{I}}$ is the unit tensor, P is the plasma thermal pressure and \mathbf{B} is the magnetic field. For simplification, we consider a fluid cell fixed at the intersection of the x -axis and magnetopause. The cell is divided into two parts, one is inside the magnetopause and the other is outside. If the density ρ is constant and the convective stress $\rho \mathbf{u} \mathbf{u}$ is ignored in the calculation, the momentum equation reduces to the pressure balance model which is also steady state with $\partial \rho \mathbf{u} / \partial t = 0$. However, if using the simulated plasma parameters on the magnetospheric side of the cell boundary, the $[\rho \mathbf{u} \mathbf{u} + \bar{\mathbf{I}}(P + B^2/2) - \mathbf{B}\mathbf{B}]$

term is always not equal on both sides of the cell, which means $\partial p_u / \partial t$ is not always equals to zero. Therefore, the cell on magnetopause is always in a dynamic state rather than fixed in time. In general, there will always be variations of the whole magnetopause. Moreover, the interchange structures rotate with Jupiter's magnetospheric system, and the number of interchange structure ejected (beyond $\sim 25 R_J$) from the magnetodisc varies with time. The radial dynamic pressure of each interchange structure varies significantly. Due to the large range of magnitude of the dynamic pressure, and the different radial transport times and assembly times of different interchange structures, the magnetopause variation range is also very large.

It is important to note that other factors may also affect the location of the Jovian magnetopause, which requires further study. For example, we have not yet implemented the hot plasma population in our global simulations, which may result in an even more dynamic Jovian magnetopause by enhancing the plasma pressure in the outer magnetosphere, and further improve the prediction of the Jovian magnetopause. It is interesting to note that the simulated plasma β in the equatorial magnetosphere beyond $45 R_J$ can reach the order of 10^2 even without the hot plasma, raising questions as to the relative importance of the hot plasma population. We expect that high-latitude region of the Jovian magnetosphere is likely influenced more when the hot plasma population is implemented. Future studies about the role of the hot plasma population are required. It is worth mentioning that in our simulation, the mass loading rate is constant while in the real system, the volcanic activity of Io is non-steady. Changes in the mass loading rate may also influence the evolution of interchange structures which should also be considered in future studies.

Data Availability Statement

The model outputs used to generate the figures for analysis presented in this paper are publicly available online (<https://doi.org/10.17605/OSF.IO/J83T7>).

Acknowledgments

This work is supported by the Excellent Young Scientists Fund (Hong Kong and Macau) of the National Natural Science Foundation of China (Grant 41922060) and the RGC General Research Fund (Grants 17300719, 17315222, and 17308520). Zhonghua Yao acknowledges the Key Research Program of the Institute of Geology & Geophysics CAS (Grant IGGCAS-201904). William R. Dunn is supported by STFC Ernest Rutherford Fellowship ST/W003449/1.

References

- Achilleos, N., André, N., Blanco-Cano, X., Brandt, P. C., Delamere, P. A., & Winglee, R. (2015). 1. Transport of mass, momentum and energy in planetary Magnetodisc regions. *Space Science Reviews*, 187(1–4), 229–299. <https://doi.org/10.1007/s11214-014-0086-y>
- Achilleos, N., Guio, P., Hardy, F., Paranicas, C., & Sorba, A. M. (2021). The Magnetodisc regions of Jupiter and Saturn. *Geophysical Monograph Series*, 29, 453–469. <https://doi.org/10.1002/9781119815624.ch29>
- Alexeev, I. I., & Belenkaya, E. S. (2005). Modeling of the Jovian magnetosphere. *Annales Geophysicae*, 23(3), 809–826. <https://doi.org/10.5194/angeo-23-809-2005>
- Aoyama, T., & Oya, H. (1985). Dawn-dusk asymmetry and spongy nature of the Jovian magnetosphere. *Journal of Geomagnetism and Geoelectricity*, 37(9), 839–867. <https://doi.org/10.5636/jgg.37.839>
- Bagenal, F., Adriani, A., Allegrini, F., Bolton, S. J., Bonfond, B., Bunce, E. J., et al. (2017). Magnetospheric science objectives of the Juno mission. *Space Science Reviews*, 213(1–4), 219–287. <https://doi.org/10.1007/s11214-014-0036-8>
- Bagenal, F., & Delamere, P. A. (2011). Flow of mass and energy in the magnetospheres of Jupiter and Saturn. *Journal of Geophysical Research*, 116(A5), A05209. <https://doi.org/10.1029/2010JA016294>
- Bame, S. J., Barraclough, B. L., Feldman, W. C., Gislis, G. R., Gosling, J. T., McComas, D. J., et al. (1992). Jupiter's magnetosphere: Plasma description from the Ulysses flyby. *Science*, 257(5076), 1539–1543. <https://doi.org/10.1126/science.257.5076.1539>
- Bonfond, B., Yao, Z. H., Gladstone, G. R., Grodent, D., Gérard, J.-C., Matar, J., et al. (2021). Are dawn storms Jupiter's auroral substorms? *AGU Advances*, 2(1), e2020AV000275. <https://doi.org/10.1029/2020AV000275>
- Chané, E., Saur, J., Keppens, R., & Poedts, S. (2017). How is the Jovian main auroral emission affected by the solar wind? *Journal of Geophysical Research: Space Physics*, 122(2), 1960–1978. <https://doi.org/10.1002/2016JA023318>
- Connerney, J. E. P., Timmins, S., Herceg, M., & Joergensen, J. L. (2020). A Jovian magnetodisc model for the Juno era. *Journal of Geophysical Research: Space Physics*, 125(10), e2020JA028138. <https://doi.org/10.1029/2020JA028138>
- Delamere, P. A., & Bagenal, F. (2010). Solar wind interaction with Jupiter's magnetosphere. *Journal of Geophysical Research*, 115(A10), A10201. <https://doi.org/10.1029/2010JA015347>
- Desroche, M., Bagenal, F., Delamere, P. A., & Erkaev, N. (2012). Conditions at the expanded Jovian magnetopause and implications for the solar wind interaction. *Journal of Geophysical Research*, 117(A7), A07202. <https://doi.org/10.1029/2012JA017621>
- Dunn, W. R., Gray, R., Wibisono, A. D., Lamy, L., Louis, C., Badman, S. V., et al. (2020). Comparisons between Jupiter's X-ray, UV and radio emissions and in-situ solar wind measurements during 2007. *Journal of Geophysical Research: Space Physics*, 125(6), e2019JA027222. <https://doi.org/10.1029/2019JA027222>
- Ebert, R. W., Bagenal, F., McComas, D. J., & Fowler, C. M. (2014). A survey of solar wind conditions at 5 AU: A tool for interpreting solar wind-magnetosphere interactions at Jupiter. *Frontiers in Astronomy and Space Sciences*, 1, 4. <https://doi.org/10.3389/fspas.2014.00004>
- Engle, I. M., & Beard, D. B. (1980). Idealized Jovian magnetosphere shape and field. *Journal of Geophysical Research*, 85(A2), 579. <https://doi.org/10.1029/JA085iA02p00579>
- Feng, E., Zhang, B., Yao, Z., Delamere, P. A., Zheng, Z., Brambles, O. J., et al. (2022). Dynamic Jovian magnetosphere responses to enhanced solar wind ram pressure: Implications for auroral activities. *Geophysical Research Letters*, 49(19), e2022GL099858. <https://doi.org/10.1029/2022GL099858>
- Grodent, D., Bonfond, B., Yao, Z., Gérard, J.-C., Radioti, A., Dumont, M., et al. (2018). Jupiter's aurora observed with HST during Juno orbits 3 to 7. *Journal of Geophysical Research: Space Physics*, 123(5), 3299–3319. <https://doi.org/10.1002/2017JA025046>

- Gu, W. D., Yao, Z. H., Pan, D. X., Xu, Y., Zhang, B., Delamere, P. A., et al. (2023). Hourly periodic variations of ultralow-frequency (ULF) waves in Jupiter's magnetosheath. *Journal of Geophysical Research*, *128*(2), e2022JE007625. <https://doi.org/10.1029/2022JE007625>
- Hardy, F., Achilleos, N., & Guio, P. (2020). Magnetopause compressibility at Saturn with internal drivers. *Geophysical Research Letters*, *47*(10), e2019GL086438. <https://doi.org/10.1029/2019GL086438>
- Hospodarsky, G. B., Kurth, W. S., Bolton, S. J., Allegrini, F., Clark, G. B., Connerney, J. E. P., et al. (2017). Jovian bow shock and magnetopause encounters by the Juno spacecraft. *Geophysical Research Letters*, *44*(10), 4506–4512. <https://doi.org/10.1002/2017GL073177>
- Huddleston, D. E., Russell, C. T., Kivelson, M. G., Khurana, K. K., & Bennett, L. (1998). Location and shape of the Jovian magnetopause and bow shock. *Journal of Geophysical Research*, *103*(E9), 20075–20082. <https://doi.org/10.1029/98JE00394>
- Huscher, E., Bagenal, F., Wilson, R. J., Allegrini, F., Ebert, R. W., Valek, P. W., et al. (2021). Survey of Juno observations in Jupiter's plasma disk: Density. *Journal of Geophysical Research: Space Physics*, *126*(8), e2021JA029446. <https://doi.org/10.1029/2021JA029446>
- Jackman, C. M., & Arridge, C. S. (2011). Solar cycle effects on the dynamics of Jupiter's and Saturn's magnetospheres. *Solar Physics*, *247*(1–2), 481–502. <https://doi.org/10.1007/s11207-011-9748-z>
- Jia, X., Hansen, K. C., Gombosi, T. I., Kivelson, M. G., Tóth, G., DeZeeuw, D. L., & Ridley, A. J. (2012). Magnetospheric configuration and dynamics of Saturn's magnetosphere: A global MHD simulation. *Journal of Geophysical Research*, *117*(A5), A05225. <https://doi.org/10.1029/2012JA017575>
- Joy, S. P., Kivelson, M. G., Walker, R. J., Khurana, K. K., Russell, C. T., & Ogino, T. (2002). Probabilistic models of the Jovian magnetopause and bow shock locations. *Journal of Geophysical Research*, *107*(A10), 1309. <https://doi.org/10.1029/2001JA009146>
- Khurana, K. K. (1997). Euler potential models of Jupiter's magnetospheric field. *Journal of Geophysical Research*, *102*(A6), 11295–11306. <https://doi.org/10.1029/97JA00563>
- Kivelson, M. G., Khurana, K., Russell, C., Walker, R., Coleman, P., Coroniti, F., et al. (1997). Galileo at Jupiter: Changing states of the magnetosphere and first looks at Io and Ganymede. *Advances in Space Research*, *20*(2), 193–204. [https://doi.org/10.1016/S0273-1177\(97\)00533-4](https://doi.org/10.1016/S0273-1177(97)00533-4)
- Krimigis, S. M., Bostrom, C. O., Keath, E. P., Zwickl, R. D., Carbary, J. F., Armstrong, T. P., et al. (1979). Hot plasma environment at Jupiter—Voyager 2 results. *Science*, *206*(4421), 977–984. <https://doi.org/10.1126/science.206.4421.977>
- Krimigis, S. M., Carbary, J. F., Keath, E. P., Bostrom, C. O., Axford, W. I., Gloeckler, G., et al. (1981). Characteristics of hot plasma in the Jovian magnetosphere: Results from the Voyager spacecraft. *Journal of Geophysical Research*, *86*(A10), 8227–8257. <https://doi.org/10.1029/JA086iA10p08227>
- Lepping, R. P., Burlaga, L. F., Klein, L. W., Jessen, J. M., & Goodrich, C. C. (1981). Observations of the magnetic field and plasma flow in Jupiter's magnetosheath. *Journal of Geophysical Research*, *86*(A10), 8141–8155. <https://doi.org/10.1029/JA086iA10p08141>
- Ma, X., Delamere, P. A., Schok, A., Wing, S., Johnson, J. R., & Liou, Y.-L. (2022). Jupiter's sheared flow unstable magnetopause boundary observed by Juno. *Journal of Geophysical Research: Space Physics*, *127*(10), e2022JA030719. <https://doi.org/10.1029/2022JA030719>
- McComas, D. J., Bagenal, F., & Ebert, R. W. (2014). Bimodal size of Jupiter's magnetosphere. *Journal of Geophysical Research: Space Physics*, *119*(3), 1523–1529. <https://doi.org/10.1002/2013JA019660>
- Merkin, V. G., & Lyon, J. G. (2010). Effects of the low-latitude ionospheric boundary condition on the global magnetosphere: Ionosphere/magnetosphere global effects. *Journal of Geophysical Research*, *115*(A10), A10202. <https://doi.org/10.1029/2010JA015461>
- Ogino, T., Walker, R. J., & Kivelson, M. G. (1998). A global magnetohydrodynamic simulation of the Jovian magnetosphere. *Journal of Geophysical Research*, *103*(A1), 225–235. <https://doi.org/10.1029/97JA02247>
- Pilkington, N. M., Achilleos, N., Arridge, C. S., Guio, P., Masters, A., Ray, L. C., et al. (2015). Internally driven large-scale changes in the size of Saturn's magnetosphere. *Journal of Geophysical Research: Space Physics*, *120*(9), 7289–7306. <https://doi.org/10.1002/2015JA021290>
- Schok, A. A., Delamere, P. A., Mino, B., Damiano, P. A., Zhang, B., Sciola, A., et al. (2023). Periodicities and plasma density structure of Jupiter's dawnside magnetosphere. *Journal of Geophysical Research*, *128*(2), e2022JE007637. <https://doi.org/10.1029/2022JE007637>
- Slavin, J. A., Smith, E. J., Spreiter, J. R., & Stahara, S. S. (1985). Solar wind flow about the outer planets: Gas dynamic modeling of the Jupiter and Saturn bow shocks. *Journal of Geophysical Research*, *90*(A7), 6275. <https://doi.org/10.1029/JA090iA07p06275>
- Stahara, S. S., Rachiele, R. R., Spreiter, J. R., & Slavin, J. A. (1989). A three dimensional gasdynamic model for solar wind flow past non-axisymmetric magnetospheres: Application to Jupiter and Saturn. *Journal of Geophysical Research*, *94*(13), 353. <https://doi.org/10.1029/JA094iA10p13353>
- Wang, Y., Yang, J., Guo, X., Wang, C., & Blanc, M. (2023). Simulation of centrifugally driven convection in Jovian inner magnetosphere using the Rice Convection Model. *Journal of Geophysical Research: Space Physics*, *128*(3), e2022JA031132. <https://doi.org/10.1029/2022JA031132>
- Wolfe, J. H., Mihalov, J. D., Collard, H. R., McKibbin, D. D., Frank, L. A., & Intriligator, D. S. (1974). Pioneer 10 observations of the solar wind interaction with Jupiter. *Journal of Geophysical Research*, *79*(25), 3489–3500. <https://doi.org/10.1029/JA079i025p03489>
- Yao, Z. H., Bonfond, B., ClarkGrodent, G. D., Grodent, D., Dunn, W. R., Vogt, M. F., et al. (2020). Reconnection- and dipolarization-driven auroral dawn storms and injections. *Journal of Geophysical Research: Space Physics*, *125*(8), e2019JA027663. <https://doi.org/10.1029/2019JA027663>
- Yao, Z. H., Grodent, D., Kurth, W. S., Clark, G., Mauk, B. H., Kimura, T., et al. (2019). On the relation between Jovian aurorae and the loading/unloading of the magnetic flux: Simultaneous measurements from Juno, Hubble Space Telescope, and Hisaki. *Geophysical Research Letters*, *46*(11), 632–11641. <https://doi.org/10.1029/2019GL084201>
- Zhang, B., Delamere, P. A., Ma, X., Burkholder, B., Wiltberger, M., Lyon, J. G., & Sorathia, K. A. (2018). Asymmetric Kelvin-Helmholtz instability at Jupiter's magnetopause boundary: Implications for corotation-dominated systems. *Geophysical Research Letters*, *45*(1), 56–63. <https://doi.org/10.1002/2017GL076315>
- Zhang, B., Sorathia, K. A., Lyon, J. G., Merkin, V. G., & Wiltberger, M. (2019). Conservative averaging-reconstruction techniques (ring average) for 3-D finite-volume MHD solvers with axis singularity. *Journal of Computational Physics*, *376*, 276–294. <https://doi.org/10.1016/j.jcp.2018.08.020>
- Zhang, B. Z., Delamere, P. A., Yao, Z. H., Bonfond, B., Lin, D., Sorathia, K. A., et al. (2021). How Jupiter's unusual magnetospheric topology structures its aurora. *Science Advances*, *7*, 15. <https://doi.org/10.1126/sciadv.abd1204>
- Zhang, B. Z., Sorathia, K. A., Lyon, J. G., Merkin, V. G., Garretson, J. S., & Wiltberger, M. (2019). GAMERA: A three-dimensional finite-volume MHD solver for non-orthogonal curvilinear geometries. *ApJS*, *244*(1), 20. <https://doi.org/10.3847/1538-4365/ab3a4c>